Journal of Nuclear Materials 168 (1989) 268–279
North-Holland, Amsterdam

ELECTRICAL CONDUCTIVITY OF POLYCRYSTALLINE URANIUM DIOXIDE

I.T. COLLIER, R.N. HAMPTON * and G.A. SAUNDERS

School of Physics, University of Bath, Claverton Down, Bath, BA2 7AY, United Kingdom

A.M. STONEHAM

Materials Physics and Metallurgy Division, AERE Harwell, Didcot, Oxon, OX11 0RA, United Kingdom

Received 17 February 1989; accepted 14 April 1989

The electrical impedance of a disc-shaped sample of polycrystalline UO_2 has been measured over a frequency range of 10 Hz to 10 MHz at temperatures between 108 and 380 K. Three distinct regions in the impedance profiles were observed; these have been associated with the region near the metallic electrodes, with the bulk material and with the grain boundaries. Activation energies for conduction have been determined in each of the three regions [0.17, 0.13 and 0.29 eV for the electrode, bulk and grain boundary contributions, respectively]. The impedance response has been modelled using a two-phase microstructure and an effective medium treatment. At low temperatures the boundary region is less conducting than the grain interior. However, at ambient temperatures and above, the boundary region dominates and electrical conduction takes place primarily through the boundaries.

1. Introduction

In the mid 1960s there was a trend to switch from Magnox-type nuclear power stations, employing metal alloy fuels, to AGR, PWR and fast reactor systems using metal oxide fuels. As a consequence, a thorough understanding of many thermophysical properties of the metal oxides became necessary. However, even after the efforts of twenty years, knowledge of the physical properties of the actinide oxide fuels is far from complete. In the future there will be interest in larger fuel burn-ups than currently used; this will drastically increase the amount of fission products present in the fuel throughout its life. There have also been proposals to introduce burnable poisons into mixed oxide fuels to modulate the power output of these systems [1]. Such proposals indicate a real need for a deep understanding of fuel properties under relevant conditions. 'In-pile' experiments have their own very technical problems, and theoretical approaches have been favoured. In many of these calculations, and also in those calculations which relate to hypothetical accidents, the electrical conductivity and derived properties are important input parameters. Consequently detailed knowledge of the electrical behaviour of urania, which in its ceramic form is the oxide on which these fuels are based, is essential for a variety of areas of further work.

Urania (UO_2) itself is a fluorite-structured oxide, with a high melting point (3120 K), and is able to exhibit very large departures from stoichiometry. Below 1400 K, in common with many other oxide ceramics, the electrical properties of urania are largely determined by the extent of the non-stoichiometry: the O/U ratio. These electrical properties (the conductivity, dielectric constant and thermoelectric power) have been extensively studied by a number of workers [2–8] for single crystal urania, and it is these quantities which provide the basic data for defect [9] and thermal conductivity [10] calculations.

Experimental data for ceramic materials are complicated because the macroscopic electrical parameters can often be perturbed by contributions from any other phases or modified regions that may be present within the material, possibly leading to distinct inter-grain and intra-grain conductivities [11]. Indeed, this is central to many applications, for example using stabilized zirconia as an oxygen sensor, where the effects of the grain

* Now at BICC Technology Centre, Wrexham, Clwyd, United Kingdom.

boundaries are paramount. An additional perturbation is that ceramics always have densities less than that of the single crystal polymorph and, this porosity need not be distributed homogeneously. The distribution of the porosity, whether inter- or intra-granularly, can have a significant effect on the electrical properties [11,12].

A technique which has been used extensively for electrical studies of ceramic materials is Complex Plane Analysis (CPA) or Impedance Spectroscopy (IS). The technique enables the measured electrical response of a system to a wide range of input frequencies to be modelled on the basis of an equivalent circuit composed of discrete components. This facilities linking of the electrical properties of each component phase to a plausible microstructure.

Hampton et al. [7,8] have studied the conductivity and dielectric constant of nominally stoichiometric single crystal UO_2 within the temperature range 80 to 1400 K using CPA. Although some studies of polycrystalline material have been carried out [2,12], they are not nearly as extensive as those for single crystal, and the observed electrical responses have not been correlated with the material microstructures. Presented here are preliminary results of investigations of the temperature dependence of the electrical impedance of a sample of polycrystalline urania. It has been possible to combine complex plane analysis with studies of the microstructure to investigate the physical basis for the electrical properties.

2. Experimental technique

The process used to acquire the electrical admittance data was straightforward: the ac admittance of disc-shaped samples was measured over a frequency range of 10 to 10^6 Hz at selected temperatures within a temperature range of 108 to 380 K. Stable sample temperatures were achieved using a nitrogen flow varistat, which enabled the temperature to be maintained to better than ± 1 K for periods between 10 and 30 min. The admittance was measured using a Hewlett Packard 4192A impedance analyser which operates by applying a constant amplitude ac voltage to the sample and determining the magnitude and phase of the resulting current, this enables the real and imaginary components of the admittance to be calculated. An advantage of this method of measuring the admittance was that the oscillator test voltage could be biased (offset) with respect to earth, enabling identification and analysis of any electrode effects (see section 3.1 and section 4.1). The impedance analyser was microcomputer-controlled, which facilitated rapid data acquisition and analysis. An example would be that, at each temperature, measurements were taken at 140 set frequencies for 5 selected bias voltages, and at each frequency data were collected and averaged over 10 readings.

Numerous descriptions of CPA have been given elsewhere [7,8,11,13]. In essence, the technique used for the analysis of the data involves the real and imaginary parts of complex quantities being plotted as a frequency dispersion at each selected temperature and bias voltages. The important feature of CPA is that the same data can be displayed in a number of alternative modes (impedance, admittance, complex capacitance $[C^* = 1/j\omega Z^*]$ and complex modulus $[M^* = j\omega Z^*]$). These representations can highlight different features and an equivalent circuit of the material may be deduced. Measurements at selected temperatures allow the determination of the temperature dependence of the resistances and capacitances. This facilitates analysis of the thermal activation of the dielectric constants and conductivities for the various components of the equivalent circuit corresponding to the sample.

The stoichiometry of the sample has not been determined explicitly; however, material that has been reduced in free-flowing hydrogen in exactly the same manner as the sample used here was found to have an O/U ratio of 2.02. The history of the sample used allows us to say, with some certainty, that the sample was hyper-stoichiometric.

3. Complex plane profiles

Examination of the data in the complex impedance representation (fig. 1) at a number of temperatures and voltages reveals three distinct regions. These three regions are also clearly identifiable in the complex admittance and capacitance representations, figs. 2 and 3.

3.1. Electrode layer

The low frequency portions (i.e. at large values of Z') of the profiles show a significant voltage dependence. The effect of increasing the bias voltage is to decrease the low frequency intercept on the abscissa and the magnitude of the peak: this suggests that in this region the resistance extracted from the Z' intercept is highly non-ohmic. This behaviour is also clearly demonstrated in fig. 3: where the electrode capacitance (the low frequency C' intercept) is voltage dependent. The voltage dependent part of the profile can be identified, physically, as being due to an electrode polarization

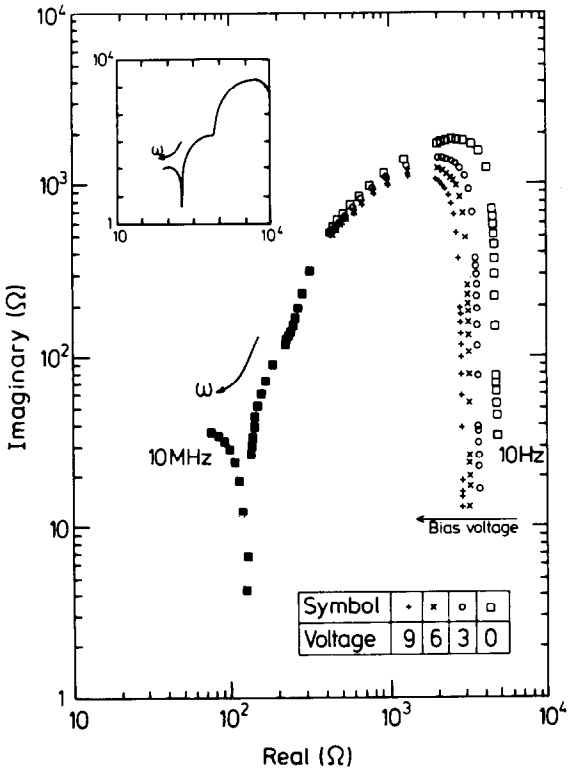

Fig. 1. Complex impedance profiles of polycrystalline UO_2 at 250 K for different applied voltages (□, 0 V; ●, 3 V; ×, 6 V; +, 9 V]. The insert shows a calculated impedance profile using the circuit in fig. 4 and component values extracted from the intercepts of the measured profile.

effect [7,11,13]. The effect of the voltage on both the resistance and capacitance can be interpreted as being due to a dependence of the effective barrier height on the applied voltage. Further consideration of this effect is given in section 4.1.

3.2. Bulk region

Comparison with CPA data for single crystal material [7] suggests that the high frequency voltage independent portion of the profile (i.e. low Z' values) contains information on the bulk properties of the material. The identification of this region can be verified from the magnitude of the corresponding capacitance intercept in the complex capacitance representation, which corresponds to a dielectric constant of 22.5. This value is somewhat lower than that normally expected for single crystal stoichiometric UO_2 ($\epsilon = 24$) though this may simply be a result of the sample porosity or to a small

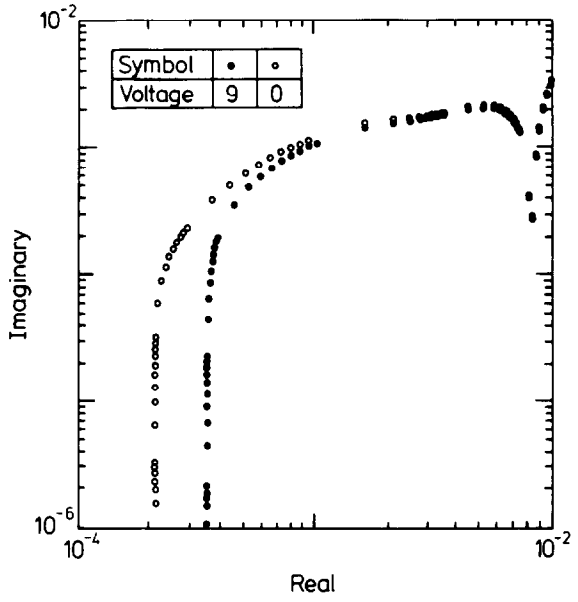

Fig. 2. Complex admittance profiles of polycrystalline UO_2 at 250 K for different applied voltages [○, 0 V; ●, 9 V].

change in stoichiometry [3]. In fact it is shown in section 4.2 that 22.5 is exactly the value that would be expected for a material with a dielectric constant equal to 24 and with the observed porosity of 7%.

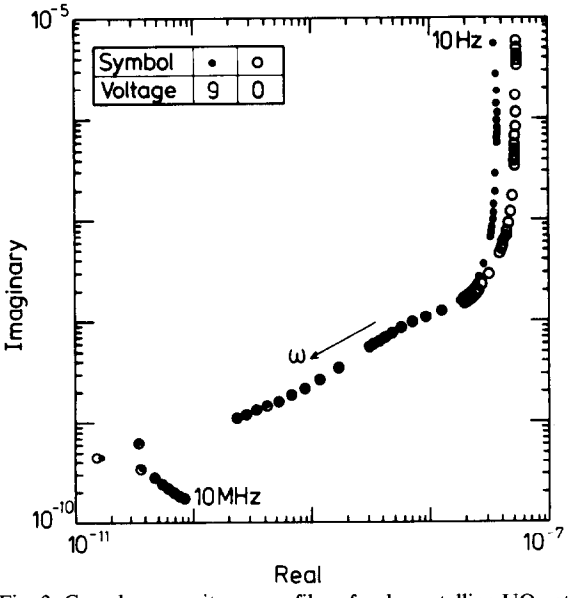

Fig. 3. Complex capacitance profiles of polycrystalline UO_2 at 250 K for different applied voltages [○, 0 V; ●, 9 V].

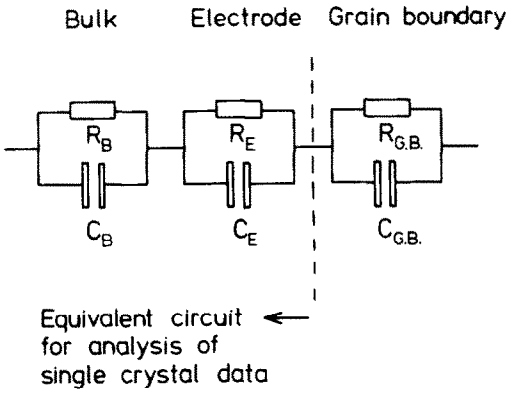

Fig. 4. Equivalent circuit used for the analysis of the impedance, admittance and capacitance profiles. Identification of the circuit elements is given in the text.

3.3. Grain boundary region

We consider that the third region of the impedance profiles, at intermediate frequencies, is due to grain boundary effects. Even though the polycrystalline material has significant porosity (7%), it is most unlikely that this, on its own, would be able to cause the formation of this intermediate feature. It is possible that the spatial distribution of the porosity may perturb the resistances and hence the magnitude of the two (bulk and grain boundary) impedance features (section 4.2). It is much more plausible that the cause is what may be thought of as an extra region with different electrical properties within the material [11]. The key features of grain boundaries are discussed further in section 4.3.

3.4. Establishment of the equivalent circuit

The basic electrical parameters (electrical conductivity and dielectric constant) of each portion of the ac impedance or admittance can only be extracted from the data if a suitable equivalent circuit can be established. Hampton et al. [7], in their studies of the ac admittance of single crystal UO_2, discovered a dual semicircular profile which was interpreted with a circuit consisting of two parallel combinations of resistors and capacitors joined in series (fig. 4). Intuitively, an equivalent circuit for the polycrystalline material must, at the very least, contain three capacitive and three resistive elements associated with the presence of the three semicircular features. The simplest standard circuit that fulfils this requirement is that of three parallel circuit elements connected in series (fig. 4). Equivalent circuits on their own are abstract networks and, for them to be of any practical use, their components need to be correlated with physically realistic mechanisms. Tentatively, at this stage, R_E and C_E can be attributed to an electrode layer, R_B and C_B to the bulk of the material and R_{GB} and C_{GB} to the grain boundaries. The insert in fig. 1 shows a calculated impedance profile using the circuit of fig. 4 with component values (R_E, C_E, R_B, C_B, R_{GB} and C_{GB}) estimated from the measured impedance response at 250 K. The agreement between measured and calculated profiles indicates that the circuit shown in fig. 4 provides a good description of the material.

4. Interpretation of profiles

Now that there is a suitable model for analysis, resistances R_B, R_{GB} and R_E can be extracted reliably from the Z' intercepts of the three regions. It is clear from the complex profiles that these intercepts are dependent upon temperature, and this is probably due to thermal activation of the equivalent circuit resistances. These (thermally-activated) resistances were used

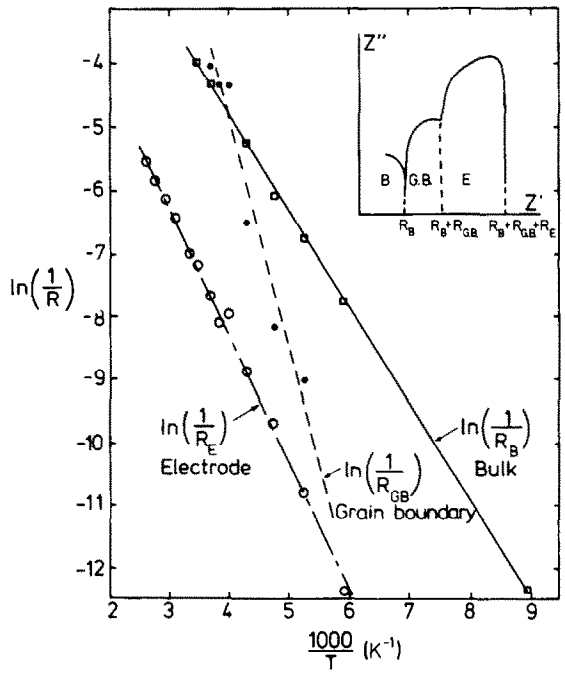

Fig. 5. An Arrhenius plot of the equivalent circuit resistances extracted from the impedance profiles assuming the circuit of fig. 4. The insert identifies the physical origins of the regions exhibited in the impedance profiles.

Table 1
Activation energies and conductivity prefactors for the bulk, grain boundary and electrode region for polycrystalline UO_2. The conductivity prefactors for the electrode region are calculated for a temperature of 272 K and those of the grain boundary region using eq. (6) and assuming a dielectric constant of 24

	$\sigma T = \sigma_0 \exp[-E_A/kT]$		$\sigma = \sigma_0 \exp[-E_A/kT]$	
	σ_0 (K^{-1} m^{-1})	E_A (eV)	σ_0 (K^{-1} m^{-1})	E_A (eV)
Bulk	1.2×10^4	0.14	25	0.13
Grain boundary	1.2×10^5	0.31	197	0.29
Electrode layer	3.7	0.19	5×10^{-3}	0.17

in conjunction with the equivalent circuit to calculate CPA profiles and their temperature dependences. Good qualitative and quantitative agreement exists between the measured and calculated CPA profiles at selected temperatures, and this agreement lends further support to the choice of circuit.

Most workers calculate activation energies and conductivity prefactors assuming small polaron conduction in which

$$\sigma T = \sigma_0 \exp[-E_A/kT]. \quad (1)$$

This has been accepted for high temperatures (near 1400 K or above), where the measured activation energy is due to contributions from a hopping and a binding energy [14]. At low temperatures the hopping energy contribution to the activation energy does not provide a significant contribution when compared to the binding energy [14] and it may be more appropriate to use

$$\sigma = \sigma_0 \exp[-E_A/kT]. \quad (2)$$

This Arrhenius plot is shown in fig. 5 while activation energies for both types of analysis are given in table 1.

The Arrhenius analysis clearly shows three different activation energies associated with bulk (intra-grain), grain boundary (inter-grain) and electrode conduction. The largest activation energy is for what we label grain boundary (inter-grain) conduction. We shall now analyse each of the three regions separately.

4.1. Electrode layer capacitance

So far the voltage dependence of the electrode layer capacitance (C_E), has been used to help identify the portions of the impedance curves. However the physics resulting from the application of a conductor to the surface of the material needs to be examined further. The capacitances of the electrode layer have been extracted from the complex capacitance plots at selected voltages and temperatures, and subsequently have been analysed using a technique reported by Henisch [15]. It assumes that the layer is a Schottky barrier and enables an estimate of the electrode layer width to be made (table 2) within the temperature range 210 K to 272 K. The technique involves calculating $dV/d(C/A)^{-2}$ and plotting this against $\epsilon_0\epsilon_r/(C/A)$ (see fig. 6); the value of ϵ_r (= 22.5) is calculated from the high frequency C' intercept of the capacitance profile. The voltage (V) is not simply the voltage applied across the specimen but is the voltage across the barrier, which needs to be calculated using the bulk, grain boundary and barrier resistances. The inherent errors are quite significant, and so the approach can only be regarded as giving an order of magnitude for the layer thickness and indicating any possible thermal effects. Notwithstanding these problems, the calculations show that the electrode layer thickness decreases with increasing temperature (insert in fig. 6). We can estimate the electrode layer conductivity at 250 K as approximately 10^{-6} Ω^{-1} m^{-1}.

Table 2
Temperature dependence of the electrode layer thickness (see section 4.1 and insert in fig. 6)

Temperature (K)	L (μm)	$L(T)^{1/2}$
210	1.50	21.7
230	1.38	20.9
250	1.29	20.4
272	0.90	14.8

Analysis of the electrode layer has used the assumption of a charge separation across a thin layer of material. In this case, we would expect the average layer thickness L to vary inversely as the square root of the temperature [16]. Table 2 shows this is reasonable for the lower temperatures; the discrepancy at 272 K may be a result of the complicating effects of the lead resistance in this range. If L is a Debye–Hückel screening length, then we can deduce cZ^2, with c the number of charges [Ze] per molecular unit of UO_2. We find that cZ^2 is 0.2, i.e. one charge per 5 molecular units if

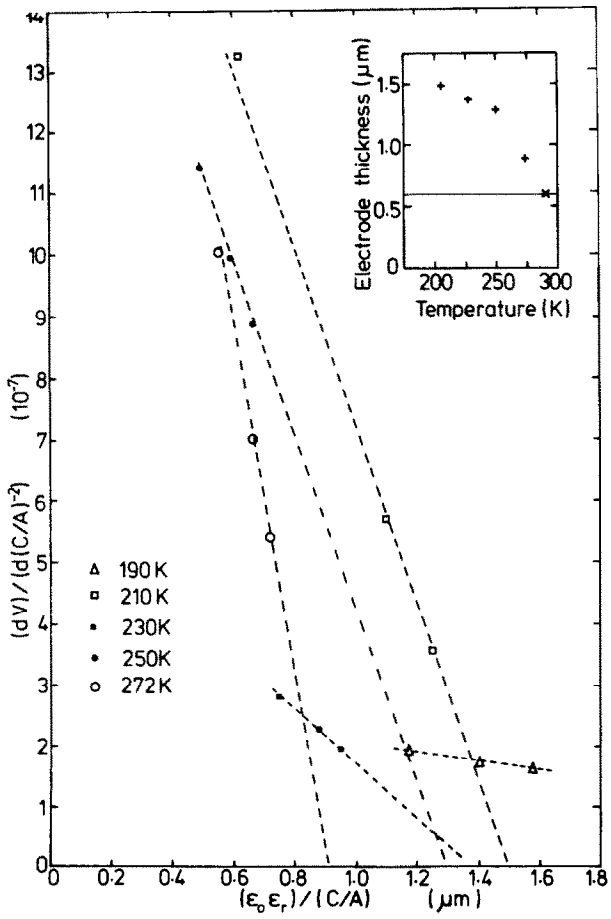

Fig. 6. Plot of $dV/d(C/A)^{-2}$ versus $\epsilon_0\epsilon_r/(C/A)$ at selected temperatures. The insert indicates the approximate dependence of electrode layer thickness with temperature. The solid line of the insert represents the level estimated from data given in ref. [7].

$Z = 1$, or one per 20 units if $Z = 2$. These are high concentrations, but they do suggest that a space-charge layer is a good description of the observed electrode contribution. At this stage there is no indication of why the observed activation energy is higher than that for the bulk.

4.2. Bulk region: the effect of porosity

The static dielectric constant for the bulk material was calculated from the high frequency C' intercept of the capacitance profile giving $\epsilon_r = 22.5$. Though this is somewhat lower than would be expected for single crystal stoichiometric UO_2, Huntley [12] has shown that (in common with many other ceramic materials [11]) polycrystalline urania exhibits a dependence of its electrical properties, specifically the dielectric constant upon porosity. Huntley measured a dependence of the dielectric constant of a urania sample held at 77 K. A complication with his work was that the sample stoichiometry could not be kept constant over the whole range of porosities. We may however assume that at low porosities, i.e. for highly dense samples, the stoichiometries remained reasonable constant. The data were analysed using a number of equations proposed for mixed conductors, though by inspection the data at low porosities were best fitted by an equation given by Maxwell [17].

$$\epsilon_m = \epsilon_2\left[1 - \frac{3(\epsilon_2 - \epsilon_1)P}{(\epsilon_1 + 2\epsilon_2) + (P(\epsilon_2 - \epsilon_1))}\right], \qquad (3)$$

where
ϵ_2 = dielectric constant of medium,
ϵ_1 = dielectric constant of void,
ϵ_m = measured dielectric constant,
P = porosity.

For UO_2 the sample density was measured, using Archimedes principle, as 10.27×10^{-3} kg m^{-3} compared with 11.04×10^{-3} kg m^{-3} for single crystal material, which gives a porosity of 7%. A simplistic approach is to assume that all of the porosity is distributed within the grains and that the voids are empty and then to set ϵ_1 to 1. Substituting values of ϵ_2 into the equation and setting ϵ_m to 22.5 allows the zero porosity dielectric constant to be estimated as ϵ_2 equal to 24.9. This value is in good agreement with values previously measured for single crystal UO_2 [3–5,7].

Electron micrographs show that the assumption of isotropic porosity wholly within the grains is not really valid, and a significant percentage is provided by the mismatch between the packing of the grains. This introduces the possibility that the total grain surface area may be larger than that calculated as the grain boundary fraction from the ratio of the capacitances of section 4.3.1 (eq. (4)). Brailsford and Hohnke [18] noted that when $\sigma_{GB} \gg \sigma_B$ the importance of this spatial distribution of the pores to the measured conductances is enhanced. A more significant effect occurs for a sample of identical porosity in which the voids appear at the grain boundaries as opposed to those in which it is distributed within the grains.

4.3. Grain boundary region: Correlation with model microstructure

The effects of two phase structures upon complex plane profiles are usually analysed in terms of either layer models or using effective medium theorems (cf eq. (3)). Conceptually, layer models are easier to relate to equivalent circuits and we will consider these models first.

4.3.1. Layer models

The grain interior phase and grain boundary phase can be present in two ways, namely either (1) a second phase completely enveloping the grains or (2) a single phase but with a constriction localised at the point linking the grains (refered to as easy paths). Work on the LISICON system [19] showed identical activation energies for the bulk and grain boundary portions of the CPA profiles; this was attributed to a constriction effect. As the activation energies are different (section 4, table 1), it is unlikely that the boundaries are produced by a constriction effect; therefore it can be assumed that there is a second phase enveloping the grains.

Macdonald [11] has reviewed a number of models for the effect of microstructure on CPA profiles. The 'brick layer' model is shown schematically in fig. 7i, in which cubic grains of side D are surrounded by a second phase of thickness $d (d \ll D)$. Two limiting cases for one-dimensional current flow are apparent: it may be either along the grain boundaries, or through the grains and then across the grain boundaries (figs. 7ii and iii respectively). Which of these dominates will depend on the relative magnitudes of the conductances g_{GB} and g_{GI}. If the current is carried along the grain boundaries, then only one arc will be observed in the impedance or modulus spectra. As may be expected the alternative conduction path, which includes two material phases, gives dual arcs in the impedance or modulus spectra. Thus the total conductivity can be analysed using two series connected parallel elements in which the components of the equivalent circuit are then weighted in terms of the fraction of the total volume occupied by the grain boundaries (X_{GB}). In this and all further analysis the term total conductivity will be used to represent the conductivity measured by a dc four-terminal pair method ie the macroscopic conductivity without a contribution from electrode impedances.

The complex profiles which represent the total macroscopic conductivity (fig. 1) have dual impedance arcs, which lends support to the 'brick layer' model with conduction through the grains and then across the grain

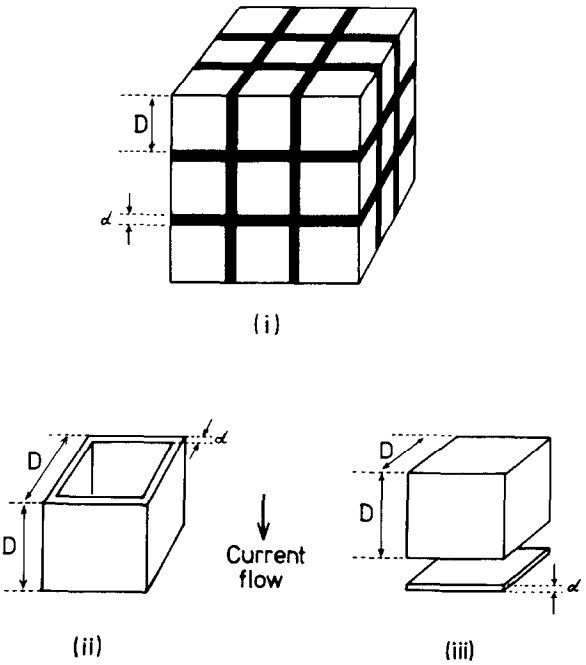

Fig. 7. (i) A schematic representation of the brick-layer model, two phase microstructure. Figs. (ii) and (iii) show the two limiting cases for one-dimensional current flow through the boundary phase only and conduction through grains and boundary phases respectively.

boundaries. For such a system it is possible to obtain crude estimates of some of the microstructural properties from the measured electrical properties [11,20]. The two key parameters are the fraction of the total volume occupied by the boundary phase or grain boundary volume fraction, X_{GB};

$$X_{GB} = 3\left[\frac{C_{GI}}{C_{GB}}\frac{\epsilon_{GB}}{\epsilon_{GI}}\right] \tag{4}$$

and the ratio of grain boundary thickness, d, to grain size D;

$$\frac{d}{D} = \left[\frac{C_{GI}}{C_{GB}}\frac{\epsilon_{GB}}{\epsilon_{GI}}\right]. \tag{5}$$

In these expressions, C_{GI} and C_{GB} are the inter-grain and intra-grain boundary capacitances, ϵ_{GI} and ϵ_{GB} are the inter-grain and intra-grain boundary static dielectric constants, D is the grain size and d is the thickness of the enveloping boundary phase. In this analysis the effect of porosity is not considered (section 4.2). We have data for C_{GB}, C_{GI} and ϵ_{GI}, but what value to take for ϵ_{GB} presents a problem. Normal practice is to assume that the two dielectric constants (ϵ_{GI} and ϵ_{GB})

are equal. However, in urania there can be significant deviations from stoichiometry [3] which effect the dielectric constant. Induced oxygen tracer diffusion work has shown that anion diffusion occurs along the grain boundaries at a different rate than for the bulk material [21], providing a plausible mechanism for achieving different stoichiometries and hence activation energies for the grain interiors and encapsulating phases. Fluorite structured urania (UO_{2+x}) exhibits a large degree of non-stoichiometry and undergoes a structural phase transition to U_4O_9 for $x = 0.25$. The dielectric constant of U_4O_9 is approximately 100 [3]. This sets an upper limit for the grain boundary dielectric constant; thus to enable an estimate of the microstructural properties, we require that the grain boundary dielectric constant is within the range:

$$\epsilon(UO_2) = 24 < \epsilon_{GB} < 100 = \epsilon(U_4O_9).$$

This gives us a range of values for the grain boundary volume fraction:

$$1.5\% < X_{GB} < 6.25\%.$$

Scanning electron micrographs of the sample established the average value for the grain size (D) to be 8 μm. This provides a range of values for the effective grain boundary thickness, d:

$$0.04\ \mu\text{m} < d < 0.17\ \mu\text{m}.$$

This value implies that the electrical response may be modelled using a second phase of this thickness. The spatial extent of the mismatch between the grains could conceivably be smaller than this as charge separation might occur at the grain boundaries.

The range of grain boundary fractions calculated from eq. (4) allows us to calculate suitable values for the conductivity prefactor of the grain boundary phase, which is of more practical use than the admittance prefactor, using the method suggested by Van Dijk and Burggraaf [20]:

$$\sigma_{0(GB)} = lX_{GB}/3Z_0A, \qquad (6)$$

where A and l are the area and thickness of the sample, respectively. The grain boundary data and the sample dimensions give

$$\sigma_{0(GB)} = X_{GB} \times 1.3 \times 10^4 (\Omega^{-1}\ \text{m}^{-1}).$$

This formulation coupled with the activation energies given in table 1 allows for the ratio of σ_B/σ_{GB} over a range of temperatures at selected grain boundary fractions to be calculated from the measured data (fig. 8). The figure shows that at low temperatures the grains are significantly more conducting than the boundaries, whereas at still higher temperatures the conductivities

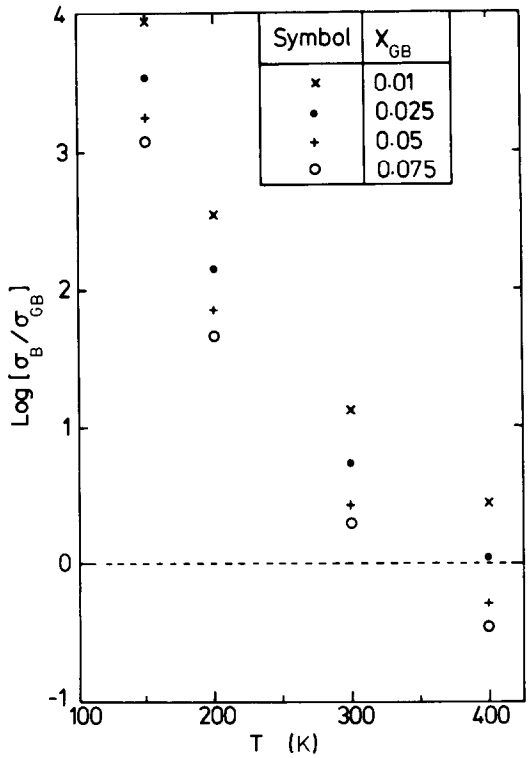

Fig. 8. Plot of σ_B/σ_{GB} versus temperature for different grain boundary volume fractions, calculated using the data given in table 1 at selected values of X_{GB} using eq. (3).

achieve parity with the boundaries exhibiting a higher conductivity than the grain. Thus at low temperatures the assumption of conduction through the grains and across the boundary fig. 7ii appears to be valid. The situation shown in fig. 7iii will then apply at higher temperatures. The situation at intermediate temperatures has been treated by Nafe [22] in his work on thoria and zirconia based electrolytes.

The total conductivity can be calculated explicitly by summing the resistances (fig. 9) of the various phases in the brick-layer model. The total resistance is built up by considering the sum of the component resistances in a column in he z direction. These columns are summed in the y direction to form a slab and similarly the slabs are combined in the z direction to give the whole sample. The total conductivity assuming conduction through the grains and across the boundaries (fig. 7ii) is given by eq.

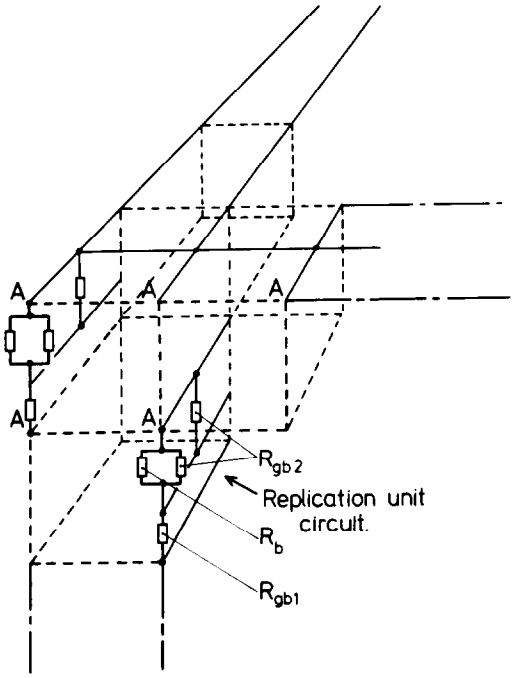

Fig. 9. The arrangement of resistances r_b, r_{gb1} and r_{gb2} (see figs. 7ii and 7iii) used in section 4.3.1., eq. (8) to calculate the total conductivity. The complete circuit is constructed by inserting the replication unit circuit at all points 'A' in space. The solid lines represent electrical short circuits.

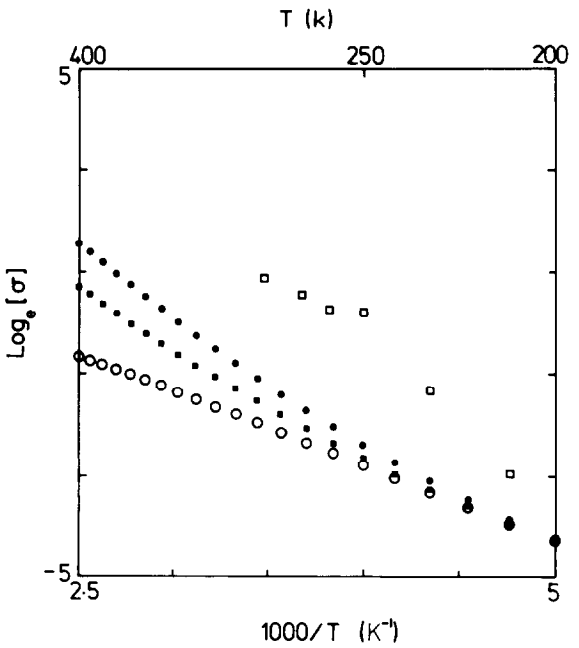

Fig. 10. Calculated values of the total conductivity of polycrystalline urania as a function of temperature at selected grain boundary fractions. Data for case 1 [○] (section 4.3.1) has been calculated using eq. (7) with $X_{GB} = 3\%$ and 5%. Data for case 2 has been calculated using eq. (8) using $X_{GB} = 3\%$ [■] and 5% [●]. Experimental data [□] extracted from complex profiles is provided for comparison.

(7) and eq. (8) takes account of conduction through the boundary phase as well (figs. 7ii and 7iii).

$$\sigma_{(\text{total 1})} = \frac{R_b + R_{gb1}}{D(1 + X_{GB}/3)}, \tag{7}$$

$$\sigma_{(\text{total 2})} = \frac{2(R_b + R_{gb1}) + R_{gb2}}{D(1 + X_{GB}/2)R_{gb2}(R_b + R_{gb1})}, \tag{8}$$

R_b, R_{gb1} and R_{gb2} are the bulk and grain boundary resistances, respectively (see fig. 9). This approach is very similar to that of Nafe [22] though a contribution R_{gb3} has not been considered and an extra contribution of R_{gb1} has been included in the z direction at each grain; for further details refer to fig. 1 and eq. (1) of ref. [22].

The data given in table 1 have been used to parameterise the effect of temperature on the component resistances; thus the conductivity at any selected temperature or grain boundary fraction may be calculated. A correction to the grain boundary conductivity needs to be applied at each value of grain boundary fraction using eq. (6). The total conductivities calculated using eqs. (7) and (8) for a range of temperatures can then be analysed by the Arrhenius approach (fig. 10 and table 3).

The first model (eq. (7)), which ignores conduction down the side of the grains, gives lower activation energies and total conductivities than the second model (eq. (8)) or the experimental data. The effect of increas-

Table 3
Calculated activation energies (eV) for different grain boundary volume fractions assuming the models in figs. 7 and 9 and eq. (8). Values have been evaluated over a temperature range of 200–400 K

X_{GB}	E_A	ln σ_0	Correlation coefficient
0.01	0.135	3.51	0.9998
0.02	0.155	4.52	0.997
0.03	0.175	5.85	0.996
0.04	0.192	6.53	0.996
0.05	0.206	7.33	0.996
0.06	0.218	8.01	0.997

Table 4
Calculated activation energies for different grain boundary volume fractions and a 50° temperature range centred at selected temperatures. The values have been calculated assuming the model in fig. 7 and eq. (7)

X_{GB}	Activation energy (eV) (for temperature range indicated)			
	350–400 K	325–375 K	300–350 K	275–325 K
0.01	0.149	0.143	0.139	0.135
0.02	0.197	0.185	0.172	0.160
0.03	0.228	0.217	0.203	0.186
0.04	0.245	0.237	0.225	0.209
0.05	0.255	0.249	0.240	0.226
0.06	0.261	0.257	0.250	0.238

ing the grain boundary volume fraction is to increase the magnitude and the activation energy of the conductivity at high temperatures. At lower temperatures it appears that only the activation energy is increased and the magnitude of the conductivity is virtually unaffected! When fitted over the whole 200° temperature range, the activation energies (table 3) are comparable with the experimental energies at the upper range of the grain boundary fraction as calculated from eq. (4). However fig. 10 shows a significant rise in the conductivity at high temperatures which is more pronounced at high boundary fractions. Calculation of the macroscopic conductivity activation energies over smaller temperature ranges (table 4) shows that the energies increase smoothly from the bulk value at low temperatures to the grain boundary value at high temperatures.

4.3.2. Effective medium theory

The layer model considered above though conceptually simple is based upon unrealistic assumptions regarding the current distribution. The effective media takes account of more realistic current distributions. They were first proposed by Maxwell [17] for dc conduction and shown to apply to ac conduction by Wagner [23]: Huntley [12] has shown this to be true empirically for low porosity UO_2. To model the macroscopic response of a two phase medium the sample is replaced with an "effective medium" in which one phase is uniformly distributed within the other. The complex conductivity for such a system is given by an expression similar to that of eq. (3). The response of the effective phase to temperature can then be calculated from the response of the component phase, in an analogous manner to that used with eqs. (7) or (8).

With UO_2 there are limiting cases for which this treatment can be applied, the first has the boundary phase isotropically dispersed in the grain phase and the second has the grain phase dispersed in the boundary phase. The macroscopic conductivity in the temperature range 200–400 K at selected grain boundary volume fractions (X_{GB}) is given in fig. 11 for both limiting cases of the theory. Macdonald [11] notes that the range of X_{GB} over which the expression is valid has not been specified though the requirement that the second phase should not perturb the field in the 'effective medium' has normally been taken to mean that the second phase is the dilute phase. However the calculations shown in fig. 11 show that 'best' agreement with experimental values occurs when the host phase in the model, is the grain boundary phase!

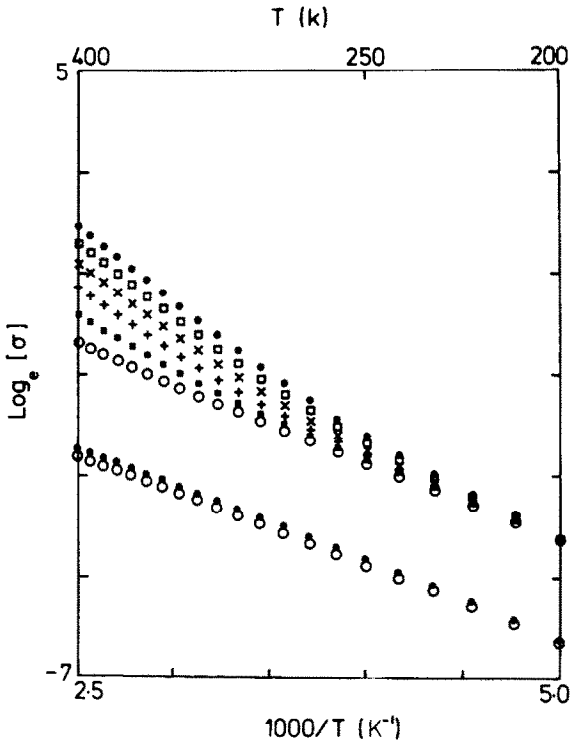

Fig. 11. The calculated values of total conductivity of polycrystalline UO_2, obtained from effective medium theory (section 4.3.2), as a function of temperature at selected grain boundary fractions: [○, 0.01; ■, 0.02; +, 0.03; ×, 0.04; □, 0.05; ●, 0.06] grain boundary dispersed in the grain phase (lower curves), grains dispersed in the grain boundary phase (upper curves). For clarity the lower curves (grain boundary dispersed in the grain phase) have been displaced downwards by 2.

4.3.3. Comparison of the two approaches

In general the data for dispersed grains in the boundary phase agree well with the explicit calculation including full contributions from the grain boundaries (eq. (8)) and the experimental data. Similarly the effective medium of boundaries dispersed in grains shows the same response as the calculation for minimal grain boundary contribution.

It is gratifying to see that two different approaches to the total conductivity problem give essentially the same results as this lends further support to the suggested microstructure and the equivalent circuit used to establish it. The question of which of the approaches discussed to use as a framework for the analysis (microstructural or effective medium) has been reviewed by Landauer [24] and is partly one of personal preference; the effective medium provides simplicity in its use whereas the microstructural approach maintains a firm link between the equivalent circuit and the physical structure of the sample.

4.3.4. Consequences of the microstructure

In practice, both of types of analysis show that the measured value of the macroscopic conductivity and its activation energy will depend critically on the grain size of the material and the exact temperature of measurement. An interesting feature is that there have been numerous values reported for the stoichiometry dominated activation energy. It can be speculated that differences between temperature ranges and grain sizes are responsible for these disparate values. In fact as long ago as 1963 Wolfe [25] and 1965 Iida [26] reported a dependence of the electrical conduction in UO_2 on the grain size.

There are three consequences of this interplay with the electrical microstructures. The first is that those thermophysical properties which depend on the electrical conduction, e.g. thermal conductivity may well be inhomogeneous. The effect of the electrical conduction on thermal conduction is given by the ambipolar contribution [10]

$$\lambda_{amb} = \frac{\sigma}{4kT}\left[\frac{U}{e}\right]^2. \tag{9}$$

However as this term is used in reactor safety analysis only to account for the thermal conductivity at temperatures near the melt, small changes in U (the energy required to disrupt the Mott insulating state; usually determined by the difference between the the activation energies above and below 1400 K) or σ caused by the microstructure may not be significant at the macroscopic scale [27]. This may not be so if one is considering effects at the microscopic scale, as would be the case when considering the effects of fission products which may segregate at grain boundaries.

The second consequence is that the macroscopic conductivity, for temperatures up to the so-called Bredig transition, will exhibit three regions: one due to the effect of the grains and grain boundaries, one due to the effect of the grain boundaries alone and one in which the conductivity is no longer dominated by deviations from stoichiometry. Single crystal material will only exhibit two regions, as it has no contributions from grain boundaries.

The third consequence is experimentally important and is that, as the grain boundary conductivity becomes increasingly more dominant, the ac electrical conduction will bypass the bulk region: CPA will not be able to resolve the two (grain and bulk) regions. The temperature at which this effect will occur will also depend upon the effect of temperature on the two dielectric constants as the factor that determines the resolution of the two features is the ratio of the time constants (CR product) and not just the conductivities.

The analysis of the microstructure in sections 4.3.1. and 4.3.2. necessitates an estimation of the range of values for the grain boundary dielectric constant. However the activation energy data of the total conductivity calculations suggest that the best match with experiment is achieved at large values of grain boundary volume fraction (X_{GB}). This in turn suggests that the value of ϵ_{GB} is closer to 100 [$\epsilon(U_4O_9)$] than 24 [$\epsilon(UO_2)$]. The most obvious mechanism for the increased value of E_{GB} is enhanced oxygen diffusion at the boundaries altering the stoichiometry at the grain edges. However this does not explain the larger activation energy for the boundaries than the bulk as the enhanced non-stoichiometry should result in a lower activation energy.

5. Conclusion

The initial work of Hampton et al. [7] on single crystal UO_2 using CPA has been successfully extended to polycrystalline material within the temperature range 108 to 380 K. This temperature range suffices to identify the several contributions and to assess their importance at higher temperatures. CPA has been able both to show the presence of, and enable extraction of quantitative data for bulk, grain boundary and electrode regions within the material. The electrical conductivities of each region are thermally activated with different values of the activation energy (0.13 eV bulk, 0.17 eV electrode, 0.29 eV grain boundary). The highly non-

ohmic effects at the metal–sample interface exhibited in single crystal material are also found in ceramic material. The physical microstructure can be well modelled by cubic grains of a bulk material, completely enveloped by a thin grain boundary layer which displays different properties to those of the bulk probably because the stoichiometry at the grain surface may not be identical to the average value of the grains. The approximate dimensions of the three regions at 270 K are 1, 8 and 0.4 μm (assuming $\epsilon = 24$) for the electrode thickness, grain size and effective grain boundary thickness respectively. At low temperatures the boundary region is much less conducting than the grain interior; the electrical microstructure is determined by both the grain interior and exterior conduction. However due to the differences in conductivity prefactors and activation energies the boundary region becomes more conducting than the bulk at ambient temperatures; microscopically the electrical conduction is determined solely by the grain exterior conduction.

Acknowledgements

The authors (I.T.C. and R.N.H.) are grateful to the Department of Energy for funding through the General Nuclear Safety Research Programme Letter and to the SERC (I.T.C.) for financial support. We wish to thank Miss S.B. Couling for carrying out the electron microscope studies.

References

[1] J.R. Mathews, J. Chem. Soc. Faraday Trans. 2, 83 (1987) 1273.
[2] J.L. Bates, Electrical Conductivity of UO_2, BNWL 296, Parts 1 and 2 (1967).
[3] J. Tateno, J. Chem. Phys. 81(12) (1984) 6130.
[4] J.D. Axe and G.D. Pettit, Phys. Rev. 151(2) (1966) 676.
[5] J. Schoenes, Phys. Rev. 63(6) (1980) 301.
[6] J.C. Killeen, J. Nucl. Mater. 88 (1980) 185.
[7] R.N. Hampton, G.A. Saunders and A.M. Stoneham, J. Nucl. Mater. 139 (1986) 185.
[8] R.N. Hampton, G.A. Saunders and A.M. Stoneham and J.H. Harding, J. Nucl. Mater. 154 (1988) 245.
[9] C.R.A. Catlow, Proc. R. Soc. London A353 (1977) 533.
[10] G.J. Hyland and J. Ralph, High Temp. High Press. 15 (1983) 179.
[11] R.J. MacDonald, Impedance Spectroscopy (Wiley, Chichester, 1988).
[12] D.J. Huntley, Can. J. Phys. 44 (1966) 2952.
[13] A.K. Jonscher, Dielectric Relaxation in Solids (Chelsea Dielectrics Press, 1983).
[14] R.N. Hampton, G.A. Saunders, J.H. Harding and A.M. Stoneham, J. Nucl. Mater. 150 (1987) 17–23.
[15] K. Henisch, Semiconductor Contacts an Approach to Ideas and Models (Clarendon Press, London, 1984).
[16] W. Hayes and A.M. Stoneham, Defects and Defect Processes in Nonmetallic Solids (Wiley, Chichester, 1985) 361, eq. (7.10).
[17] J.C. Maxwell, A Treatise on Electricity and Magnetism, 3rd Ed., Vol. 1 (1891) p. 440.
[18] A.D. Brailsford and D.K. Hohnke, Solid State Ionics 11 (1983) 133.
[19] P.G. Bruce and A.R. West, J. Electro. Chem. Soc. 130(3) (1983) 662.
[20] T. Van Dijk and A.J. Burggraaf, Phys. Status Solidi A63 (1981) 229.
[21] H. Matzke, Lattice Defects and Irradiation Damage in ThO_2, UO_2 and $(U, Pu)O_2$ in Plutonium and other Actinides (North-Holland, Amsterdam, 1976).
[22] H. Nafe, Solid State Ionics 13 (1984) 255.
[23] K.W. Wagner, Explanation of the Dielectric Fatigue Phenomenon on the Basis of Maxwell's Concept, Archive for Electrotechnik, Ed. H. Schering (Springer Verlag, Berlin, 1914).
[24] R. Landauer, Electrical Conductivity in Inhomogeneous Media, American Institute of Physics Conf. Proc. No. 40 (1978) p. 2–45.
[25] R.A. Wolfe, Electrical Conductivity and Thermoelectric Power of Uranium Divide, Tech. Rept. WAPD-270 (1963).
[26] S. Tida, Jap. J. Appl. Phys. 4(11) (1965) 833.
[27] D.M. Duffy and A.M. Stoneham, J. Phys. C16 (1983) 4087.